Research Square

Preprints are preliminary reports that have not undergone peer review.
They should not be considered conclusive, used to inform clinical practice,
or referenced by the media as validated information.

# Multi-omic profiling identifies distinct MAPK-centric subgroups in BRAF- and PTPN11-mutant IDH-wildtype glioblastoma

**Tim Vladimirov**
University Hospital Erlangen, Friedrich-Alexander-Universität Erlangen-Nürnberg
**László Bárány**
University Hospital Erlangen, Friedrich-Alexander-Universität Erlangen-Nürnberg
**Sebastian Jeising**
University Hospital Erlangen, Friedrich-Alexander-Universität Erlangen-Nürnberg
**Oliver Schnell**
University Hospital Erlangen, Friedrich-Alexander-Universität Erlangen-Nürnberg
**Daniel Delev**
University Hospital Erlangen, Friedrich-Alexander-Universität Erlangen-Nürnberg
**Dieter Henrik Heiland**
henrik.heiland@uk-erlangen.de

University Hospital Erlangen, Friedrich-Alexander-Universität Erlangen-Nürnberg

**Research Article**

**Keywords:** Glioblastoma, BRAF, PTPN11, Multi-omics

**Posted Date:** April 24th, 2026

**DOI:** https://doi.org/10.21203/rs.3.rs-9415669/v1

**License:** This work is licensed under a Creative Commons Attribution 4.0 International License.
Read Full License

**Additional Declarations:** No competing interests reported.

# Multi-omic profiling identifies distinct MAPK-centric subgroups in BRAF- and PTPN11-mutant IDH-wildtype glioblastoma

**Tim Vladimirov[1]**, Laszlo Barany[1], Sebastian Jeising[1], Oliver Schnell[1], **Daniel Delev[1]*, Dieter Henrik Heiland[1,2,3]***

Affiliations:

[1]Department of Neurosurgery, University Hospital Erlangen, Friedrich-Alexander-Universität Erlangen-Nürnberg, Erlangen, Germany

[2]Translational Neurosurgery, Friedrich-Alexander-Universität-Nürnberg-Erlangen, Erlangen, Germany

[3]Department of Neurological Surgery, Northwestern University Feinberg School of Medicine, and Malnati Brain Tumor Institute, Northwestern Medicine, Chicago, USA

*Correspondence:*

Dieter Henrik Heiland

Department of Neurosurgery

Friedrich-Alexander-Universität-Erlangen-Nürnberg

Schwabachanlage 6

91054 Erlangen

-Germany-

Tel: +49 (0) 9131 8546045

E-mail: henrik.heiland@uk-erlangen.de

**Acknowledgments**

This publication is submitted in partial fulfillment of the requirements for obtaining the degree 'Dr. med.' at the Friedrich-Alexander-Universität Erlangen-Nürnberg, Erlangen, Germany.

## Abstract

### Background

The role of MAPK pathway alterations in IDH-wildtype glioblastoma remains incompletely defined, particularly for BRAF and PTPN11 mutations.

### Methods

We performed an integrated analysis of publicly available glioblastoma datasets (n = 641; IDH-wildtype n = 588), including 25 BRAF-mutated, 22 PTPN11-mutated, and 537 double-wildtype tumors. Clinical, genomic, transcriptomic, and epigenetic features were compared across subgroups.

### Results

Clinical characteristics and overall survival did not differ between subgroups (global log-rank p = 0.60). In contrast, molecular analyses revealed distinct architectures. PTPN11-mutated tumors showed strong enrichment of RTK–RAS–MAPK signaling (OR 22.77, 95% CI 12.79–40.53, FDR < 0.001) with additional PI3K–AKT–mTOR and cell cycle activation, frequently co-occurring with NF1 alterations (68%). BRAF-mutated tumors also demonstrated MAPK enrichment (OR 4.09, 95% CI 2.21–7.56, FDR = $3.55 \times 10^{-5}$) but with a more diffuse co-mutation landscape. Transcriptomic analyses identified a hyperactivated state in BRAF-mutated tumors, marked by proliferation, inflammatory, angiogenic, and metabolic programs, whereas PTPN11-mutated tumors clustered closer to double-wildtype glioblastoma.

### Conclusions

BRAF- and PTPN11-mutant glioblastomas define distinct MAPK-centric subgroups without survival differences but with divergent molecular architectures, supporting pathway-informed stratification and therapeutic targeting.

### Keywords

Glioblastoma, BRAF, PTPN11, Multi-omics

## Introduction

Glioblastoma (GB) is the most common and biologically aggressive primary malignant brain tumor in adults, characterized by poor prognosis despite multimodal therapy. Long-term survival remains rare, with five-year overall survival below 3% [1]. A major challenge in GB management is its pronounced molecular and microenvironmental heterogeneity, which drives therapeutic resistance and limits the success of precision oncology approaches. In contrast to other malignancies such as melanoma or non-small cell lung cancer, immune checkpoint inhibition has shown minimal efficacy in GB, largely due to intrinsic and therapy-induced immunosuppressive mechanisms within the tumor microenvironment [2]. The mitogen-activated protein kinase (MAPK) signaling pathway represents a central regulator of cellular proliferation, differentiation, and survival, and is frequently dysregulated in GBs [3]. Within this pathway, *PTPN11*, encoding the non-receptor tyrosine phosphatase SHP2, plays a pivotal role by integrating signals across multiple oncogenic cascades, including RAS-RAF-MEK-ERK, PI3K-AKT, and JAK-STAT pathways. SHP2 has emerged as a context-dependent oncogenic driver, contributing to tumor growth, stemness, and immune evasion. In glioblastoma, elevated *PTPN11* expression has been observed particularly in glioma stem-like cells, where it promotes proliferation and tumorigenicity [4]. Clinically, recent genomic analyses suggest that *PTPN11* alterations occur in a subset of IDH-wildtype GB and may be associated with inferior survival, although their biological and therapeutic implications remain incompletely understood [5, 6]. Another key component of MAPK signaling is BRAF, a serine-threonine kinase downstream of RAS. Activating BRAF alterations, most prominently the V600E mutation, are well-established oncogenic drivers across multiple tumor types and represent actionable therapeutic targets [7]. In neuro-oncology, BRAF mutations are characteristic of several low-grade and circumscribed gliomas, but also occur in a subset of glioblastomas [8, 9]. Importantly, combined BRAF and MEK inhibition has demonstrated clinical activity in BRAF-mutant gliomas and is currently incorporated into treatment guidelines for selected patients. However, responses are often transient, and resistance mechanisms potentially involving adaptive cellular reprogramming and immune escape, limit long-term efficacy [10, 11]. Furthermore, the prognostic significance and molecular context of BRAF alterations in GB remain heterogeneous and incompletely defined. Despite the emerging relevance of MAPK pathway alterations in GB, PTPN11- and BRAF-driven tumors have largely been studied in isolation, and it remains unclear whether they define biologically distinct subgroups or represent overlapping oncogenic programs within IDH-wildtype GB [12]. A direct comparative analysis of these alterations, particularly in the context of co-mutation patterns, clinical characteristics, and survival outcomes, is currently lacking.

In this study, we systematically analyze BRAF- and PTPN11-mutant glioblastomas using publicly available large-scale genomic datasets, including comprehensive molecular and clinical annotations. We compare these subgroups to IDH-wildtype GB lacking these alterations to (i) define their clinical and prognostic relevance, (ii) characterize associated co-mutation landscapes, and (iii) assess whether they represent distinct molecular subtypes within GB. By integrating genomic and clinical data, this work aims to refine the stratification of MAPK-driven glioblastoma and provide a rationale for pathway-informed therapeutic strategies.

## Materials and Methods

### Patient cohort and data acquisition

Publicly available glioblastoma datasets were retrieved from the cBioPortal for Cancer Genomics [13]. The analysis included the studies gbm_columbia_2019, gbm_tcga_gdc, gbm_tcga, gbm_tcga_pub, gbm_tcga_pub2013, gbm_tcga_pan_can_atlas_2018, gbm_mayo_pdx_sarkaria_2019, and lgggbm_tcga_pub. In total, 641 glioblastoma cases were compiled, of which 588 were annotated as IDH-wild-type. Within this IDH-wild-type cohort, 25 tumors harbored BRAF mutations, 22 harbored PTPN11 mutations, and 2 showed concurrent alterations. The remaining 537 IDH-wild-type tumors without BRAF or PTPN11 mutations served as the double-wild-type reference group.

### Clinical and survival analyses

Age at diagnosis, sex distribution, and overall survival were compared across the BRAF-mutated, PTPN11-mutated, and double-wild-type IDH-wild-type glioblastoma groups. Because subgroup sizes were imbalanced and age was not normally distributed, age was analyzed using non-parametric testing. Sex distribution was assessed using contingency table analysis. Overall survival was defined as the interval from diagnosis to death or last follow-up and was analyzed using Kaplan-Meier estimates and log-rank testing. Patients with missing clinical or survival data were excluded from the respective analyses.

### Copy-number and somatic alteration analyses

Gene-level copy-number alteration data were obtained from cBioPortal, and high-level amplification was defined as a copy-number call of +2. Copy-number status for BRAF and PTPN11 was evaluated in relation to mutation status, and survival analyses were additionally stratified according to mutation and amplification categories. To characterize the molecular context of BRAF- and PTPN11-mutant glioblastomas, somatic mutation data were analyzed at the patient level using non-synonymous alterations only. Mutation frequencies were calculated for each subgroup to identify recurrently altered genes, and shared as well as subgroup-specific recurrent alterations were assessed by overlap analysis. In addition, pairwise gene-gene association analyses were performed to identify patterns of co-occurrence and mutual exclusivity among recurrent alterations.

### Pathway-level analyses

To place subgroup-specific mutation patterns into a biologically interpretable framework, recurrent alterations were mapped onto major canonical oncogenic pathways, including RTK-RAS-MAPK, PI3K-AKT-mTOR, TP53 signaling, cell cycle control, and telomere maintenance. Pathway-level enrichment and prevalence were compared between mutation-defined subgroups and the double-wild-type reference cohort.

### Oncoprint visualization

For structured comparison of mutation patterns across cohorts, a matched oncoprint was generated using representative BRAF-mutated, PTPN11-mutated, and double-wild-type cases. Matching

considered major clinical and technical variables, including age, sex, sequencing platform, and tumor status. Recurrent non-synonymous alterations were visualized at the patient level to illustrate subgroup-specific mutational landscapes.

**Transcriptomic analysis**

Bulk RNA sequencing count data for IDH-wild-type glioblastoma were obtained from TCGA together with curated clinical and molecular annotations. Differential gene expression analyses were performed for three contrasts: BRAF-mutated versus double-wild-type, PTPN11-mutated versus double-wild-type, and BRAF-mutated versus PTPN11-mutated glioblastoma. Genes were considered differentially expressed based on adjusted p value and fold-change thresholds. To identify biologically relevant transcriptional programs, preranked gene set enrichment analysis was performed using the MSigDB Hallmark gene sets.

**DNA methylation and deconvolution analyses**

Genome-wide DNA methylation data from TCGA-GBM were analyzed using Illumina HumanMethylation450 arrays. Samples were classified according to BRAF mutation status, and differential methylation analyses were performed between BRAF-mutated and BRAF-wild-type tumors. Differentially methylated CpGs were mapped to associated genes, followed by Gene Ontology enrichment analysis to identify overrepresented biological processes. In addition, methylation-based deconvolution was applied to infer relative cell-type contributions, with a particular focus on neuronal signatures. These analyses were further compared with an independent Mayo methylation cohort.

**Statistical analysis**

Statistical analyses were performed in Python and R using established scientific and Bioconductor libraries. Multiple-testing correction was applied where appropriate using the Benjamini-Hochberg method or Holm adjustment for pairwise comparisons. A two-sided p value $< 0.05$ was considered statistically significant.

## Results

### MAPK-driven glioblastomas do not differ in clinical characteristics or survival

Age at diagnosis was comparable across BRAF-mutated, PTPN11-mutated, and BRAF/PTPN11 double-wild-type IDH-wild-type glioblastomas (Kruskal-Wallis p = 0.95; all pairwise Holm-adjusted p > 0.9; **Supplementary Fig. S1, Table S1**). Similarly, sex distribution did not differ between subgroups ($\chi^2(2) = 0.81$, p = 0.67; **Supplementary Fig. S2**, **Table S2**). Median overall survival was 14.7 months for BRAF-mutated (n = 21), 16.0 months for PTPN11-mutated (n = 22), and 14.5 months for double-wild-type tumors (n = 448; **Supplementary Table S3**). Kaplan-Meier curves were largely overlapping, and no significant differences in overall survival were observed (global log-rank p = 0.60). Pairwise comparisons likewise showed no differences between BRAF-mutated and double-wild-type (p = 0.78), PTPN11-mutated and double-wild-type (p = 0.32), or BRAF-mutated and PTPN11-mutated tumors (p = 0.62; **Supplementary Fig. S3**, **Table S4**). Together, these findings indicate that MAPK pathway alterations alone do not define clinically distinct subgroups in IDH-wild-type glioblastoma.

### Distinct somatic alteration patterns in BRAF- and PTPN11-mutated glioblastomas

Copy-number amplification of *BRAF* or *PTPN11* was rare in the combined cohort, with only four *BRAF* amplification-only cases and one *PTPN11* amplification-only case. Notably, no tumors harbored concurrent mutation and amplification of the same gene (**Supplementary Tables S5-S6, Fig. S4-S5**). Consistent with this low frequency, amplification status was not associated with differences in overall survival (**Supplementary Fig. S6**). Analysis of patient-level mutation prevalence revealed distinct co-alteration landscapes across genomic subgroups (**Fig. 1A**). *BRAF*-mutated glioblastomas (n = 25) exhibited a relatively diffuse mutational profile, with the most frequent alterations observed in *TTN* and *MUC16* (each 40%), followed by *PLIN4* and *PABPC3* (36%). Additional genes were altered at moderate frequencies (~30%), without a single dominant co-driver beyond *BRAF*. In contrast, *PTPN11*-mutated tumors (n = 22) showed a more structured co-mutation pattern, dominated by *NF1* alterations (68%), followed by *TTN* (50%) and *PTEN* (36%). This pattern suggests a strong convergence on RAS/MAPK and PI3K pathway dysregulation. By comparison, double-wild-type glioblastomas (n = 537) were characterized by canonical driver alterations, including *PTEN* (36%), *TP53* (30%), *EGFR* (25%), and *NF1* (12%). Collectively, these data indicate that *BRAF*- and *PTPN11*-mutated glioblastomas are embedded within distinct molecular contexts. *PTPN11*-mutant tumors are enriched for NF1-associated signaling alterations, whereas *BRAF*-mutant tumors display a broader and less centralized co-mutation landscape.

### Overlap of recurrent alterations highlights subgroup-specific genomic programs

To assess shared versus subgroup-specific alterations, we compared recurrently altered genes across *BRAF*-mutated, *PTPN11*-mutated, and double-wild-type glioblastomas (**Fig. 1B**). Most recurrent alterations were cohort-specific, with 39 genes unique to *BRAF*-mutated tumors and 35 unique to *PTPN11*-mutated tumors. The double-wild-type cohort retained 27 exclusive genes, underscoring substantial divergence in mutational landscapes. Overlap between subgroups was limited. Eight genes were shared between *BRAF*-mutated and double-wild-type tumors, and twelve between *PTPN11*-mutated and double-wild-type tumors. Notably, no genes were uniquely shared between *BRAF*- and

*PTPN11*-mutated tumors. Only three genes (*MUC16*, *PABPC3*, and *TTN*) were common to all groups. Together, these findings indicate that *BRAF*- and *PTPN11*-mutated glioblastomas are defined by largely distinct repertoires of recurrent alterations, rather than representing minor variations within a shared genomic background.

**MAPK signaling and distinct genomic architectures define mutation-specific glioblastoma subsets**

Pathway-level analysis delineated distinct oncogenic architectures across genomic subgroups (**Fig. 1C**; **Supplementary Fig. S7**). In PTPN11-mutated glioblastomas, the RTK-RAS-MAPK pathway was strongly enriched compared with double-wild-type tumors (OR = 22.77, 95% CI 12.79-40.53, FDR < 0.001), with additional enrichment of PI3K-AKT-mTOR signaling (OR = 1.99, 95% CI 1.14-3.49, FDR = 0.0317) and cell cycle control (OR = 6.36, 95% CI 1.21-33.59, FDR = 0.039). TP53 signaling was not differentially enriched (OR = 0.93, 95% CI 0.41-2.13, FDR = 0.87). BRAF-mutated tumors also showed significant enrichment of RTK-RAS-MAPK signaling (OR = 4.09, 95% CI 2.21-7.56, FDR = $3.55 \times 10^{-5}$), but no additional pathways reached significance after multiple-testing correction, indicating limited pathway convergence beyond MAPK signaling. In contrast, double-wild-type tumors were depleted for RTK-RAS-MAPK alterations (OR = 0.17, 95% CI 0.12-0.25, FDR < 0.001) and showed no enrichment for PI3K-AKT-mTOR, TP53, cell cycle, or telomere maintenance pathways (all FDR ≥ 0.746). Overall, both BRAF- and PTPN11-mutated glioblastomas are defined by MAPK-dominant signaling, with broader pathway co-activation in PTPN11-mutated tumors, whereas double-wild-type tumors lack this enrichment pattern.

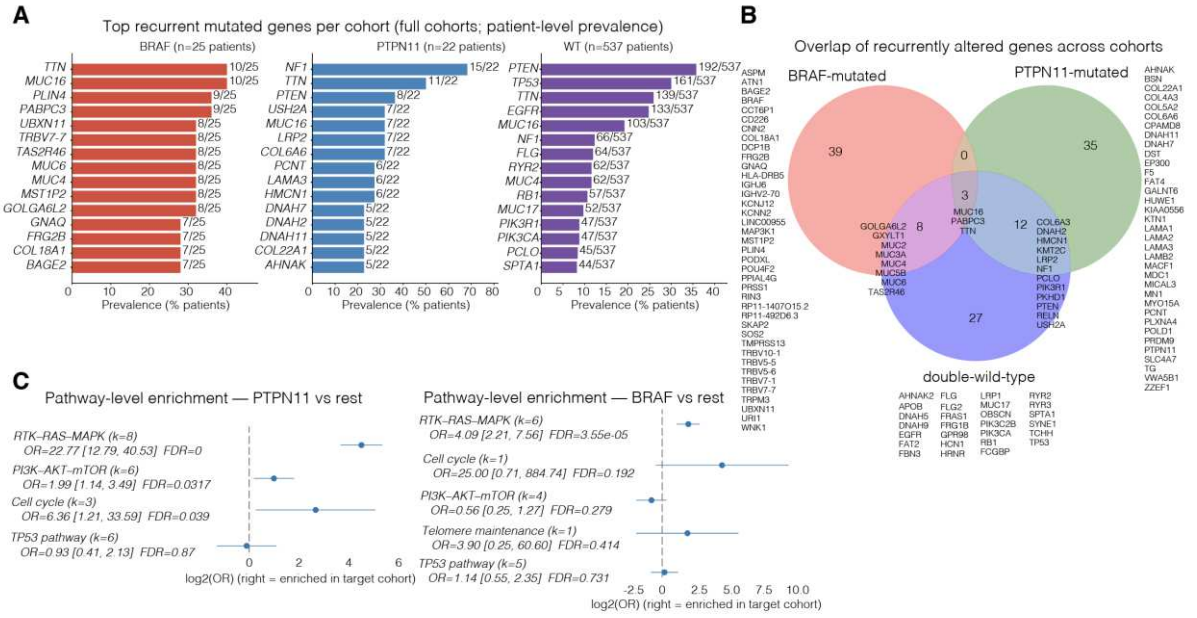



**Figure 1. Distinct mutational and pathway architectures of BRAF- and PTPN11-mutated glioblastomas.**

(A) Top recurrently mutated genes across BRAF-mutated (n = 25), PTPN11-mutated (n = 22), and double-wild-type (WT; n = 537) IDH-wild-type glioblastomas, shown as patient-level mutation prevalence. BRAF-mutated tumors exhibit a relatively diffuse mutational spectrum, whereas PTPN11-

mutated tumors are enriched for NF1 and additional pathway-related alterations. WT tumors are dominated by canonical glioblastoma drivers, including PTEN, TP53, and EGFR. (B) Overlap of recurrently altered genes across genomic cohorts. The majority of alterations are cohort-specific, with limited overlap between groups. Only three genes (MUC16, PABPC3, TTN) are shared across all cohorts, highlighting distinct mutational repertoires. (C) Pathway-level enrichment analysis comparing PTPN11-mutated and BRAF-mutated tumors to the remaining cohort. PTPN11-mutated tumors show strong enrichment of RTK-RAS-MAPK signaling, along with additional PI3K-AKT-mTOR and cell cycle pathway activation. BRAF-mutated tumors demonstrate selective enrichment of MAPK signaling without broader pathway co-activation. Effect sizes are shown as log2(odds ratios) with 95% confidence intervals; false discovery rate (FDR)-adjusted p values are indicated.

**Co-occurrence and mutual exclusivity patterns define distinct genetic architectures**

To compare mutation patterns under controlled conditions, we generated a matched oncoprint including *BRAF*-mutated, *PTPN11*-mutated, and double-wild-type glioblastomas (n = 20 per cohort), with the wild-type subset matched for age, sex, sequencing center, platform, and tumor state. BRAF-mutated tumors displayed a compact mutation architecture with moderate mutation burden, dominated by missense and truncating events and lacking extreme outliers, **Fig 2A**. In contrast, *PTPN11*-mutated tumors showed greater heterogeneity, including two hypermutated samples exceeding the interquartile range threshold. Even after excluding these from scaling, the *PTPN11* cohort exhibited broader co-alteration across recurrent genes. The double-wild-type cohort was characterized by canonical glioblastoma drivers, including *TP53* and *PTEN*, with a more uniform and intermediate mutation burden. Cohort-defining genes were excluded and highly mutable genes filtered to avoid artefacts. Under these constraints, mutation-defined subgroups remained clearly separable, with *PTPN11*-mutated tumors showing the greatest internal heterogeneity. Mutation-burden-adjusted association analysis revealed distinct interaction patterns across cohorts (**Fig. 2B**; **Supplementary Fig. S8-S9**). In the *BRAF*-mutated cohort (N = 25), recurrent genes including *RB1*, *MAP3K1*, *PLIN4*, *GXYLT1*, *PABPC3*, *GOLGA6L2*, and *TAS2R46* formed a tightly co-occurring module with multiple significant associations after FDR correction. Classical tumor suppressors such as *TP53* and *RB1* did not show strong mutual exclusivity, supporting an additive model in which secondary alterations accumulate alongside *BRAF*-driven signaling. In contrast, the *PTPN11*-mutated cohort (N = 22) exhibited a more heterogeneous architecture with both co-occurrence and mutual exclusivity patterns. Genes such as *RYR3*, *APOB*, *NF1*, and *PABPC3* showed strong co-alteration, with *NF1* highlighting convergence on RAS-MAPK signaling. Concurrent negative associations between specific gene pairs suggest the presence of distinct molecular sub-configurations within this group. In the combined cohort (N = 638), a clear separation emerged between a co-occurring module (including *PLIN4*, *MAP3K1*, *GXYLT1*, *PABPC3*, *TRBV7-7*, *TAS2R46*, and *GOLGA6L2*) and canonical glioblastoma drivers (*EGFR*, *TP53*, *RB1*, *PTEN*), supported by negative log2(odds ratio) values. This indicates partially distinct evolutionary trajectories within IDH-wild-type glioblastoma. Within the double-wild-type cohort (N = 537), co-occurrence patterns were weaker but remained structured, with associations among *GXYLT1*, *PABPC3*, *TRBV7-7*, and *TAS2R46*, and limited positive association with canonical drivers. Overall, *BRAF*- and *PTPN11*-mutated tumors

exhibit stronger and more distinct co-alteration structures, whereas the double-wild-type population shows subtler but reproducible patterns beyond mutation burden alone.

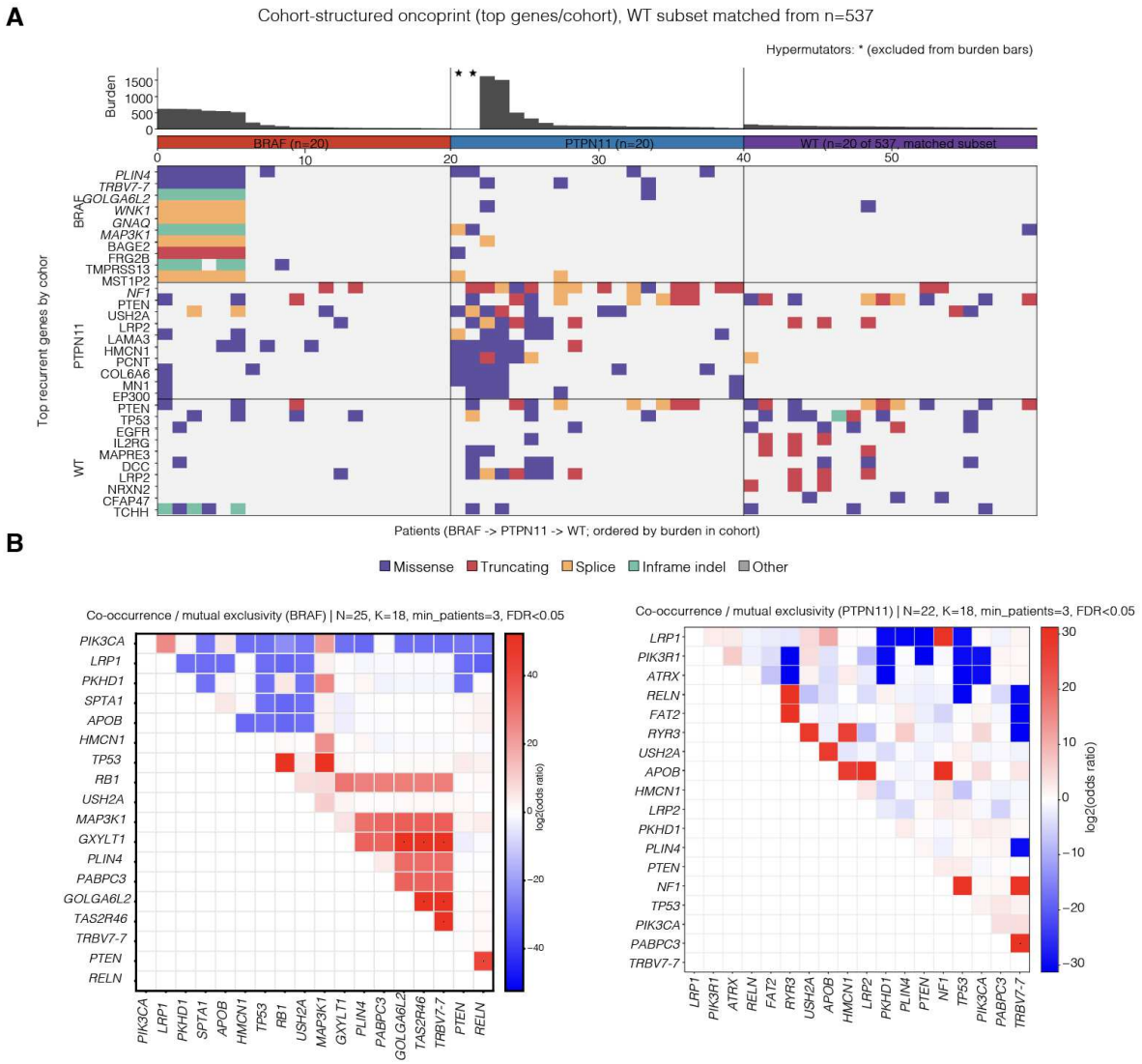



**Figure 2. Cohort-specific mutation architecture and gene-gene interaction patterns in MAPK-defined glioblastoma.**

(A) Cohort-matched oncoprint of BRAF-mutated (n = 20), PTPN11-mutated (n = 20), and double-wild-type (WT; n = 20, selected from n = 537) IDH-wild-type glioblastomas. Patients are ordered by mutation burden within each cohort. Recurrent non-synonymous alterations are displayed, with genes grouped by cohort-specific prevalence. BRAF-mutated tumors exhibit a compact mutation profile, whereas PTPN11-mutated tumors show increased heterogeneity, including hypermutated cases (asterisks). WT tumors are dominated by canonical glioblastoma drivers. Cohort-defining genes were excluded to avoid circularity. Mutation types are color-coded as indicated. (B) Pairwise co-occurrence and mutual exclusivity analysis of recurrently altered genes in BRAF-mutated (left) and PTPN11-mutated (right) glioblastomas. Heatmaps display log2(odds ratios), with red indicating co-occurrence and blue indicating mutual exclusivity. BRAF-mutated tumors show a predominantly co-occurring module of alterations, consistent with an additive mutational architecture. In contrast, PTPN11-mutated tumors

exhibit a more heterogeneous pattern with both co-occurrence and mutual exclusivity relationships, suggesting distinct sub-configurations within this subgroup. Only gene pairs meeting significance thresholds (FDR < 0.05) are shown.

**Differential expression and pathway enrichment analysis**

Pairwise differential expression analysis (**Fig. 3**) revealed the strongest transcriptional differences between BRAF-mutated and double-wild-type glioblastomas, with numerous upregulated genes in BRAF-mutated tumors (e.g., *ARG1*, *IL31RA*, *AEP*) and fewer downregulated transcripts (including *CDKN2A*, *EGFR*, *PCDHGB7*). Comparison of *BRAF*- and *PTPN11*-mutated tumors showed bidirectional changes, with BRAF-enriched transcripts such as *LINC01116* and *KIF18B* and *PTPN11*-enriched transcripts including *PCDHGB7* and *EFZF1-AS1*. In contrast, only a limited number of genes were differentially expressed between *PTPN11*-mutated and double-wild-type tumors, indicating closer transcriptional similarity between these groups. Preranked Hallmark GSEA revealed a structured pathway pattern separating *BRAF*-mutated tumors from both PTPN11-mutated and double-wild-type glioblastomas (**Supplementary Fig. S10**). *BRAF*-mutated tumors showed strong enrichment of proliferation programs (G2M checkpoint, E2F targets, mitotic spindle, MYC targets V1/V2), alongside inflammatory (TNFα/NF-κB, interferon-α/γ), angiogenic, and metabolic pathways (hypoxia, glycolysis, mTORC1, PI3K-AKT-mTOR, cholesterol homeostasis, bile acid metabolism, coagulation, complement). These pathways were largely depleted in *PTPN11*-mutated versus double-wild-type tumors. Additional pathways (IL6-JAK-STAT3, IL2-STAT5) followed the same direction with smaller effect sizes. Overall, *BRAF*-mutated glioblastomas exhibit a transcriptionally “hyper-activated” state, whereas *PTPN11*-mutated tumors show broad depletion of these programs and cluster closer to the double-wild-type baseline.

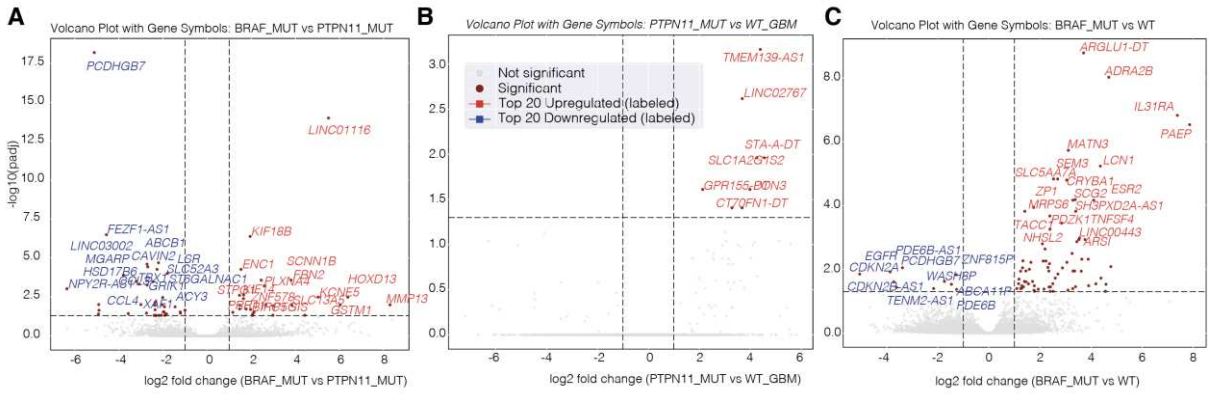



**Figure 3. Differential gene expression distinguishes BRAF-mutated glioblastomas from PTPN11-mutated and double-wild-type tumors.**

(A) Volcano plot comparing BRAF-mutated versus PTPN11-mutated glioblastomas. Differentially expressed genes show bidirectional changes, with selected top upregulated (red) and downregulated (blue) genes labeled, highlighting distinct transcriptional programs between MAPK-driven subgroups. (B) Volcano plot comparing PTPN11-mutated versus double-wild-type (WT) glioblastomas. Only a limited number of genes are significantly differentially expressed, indicating close transcriptional similarity between PTPN11-mutated and WT tumors. (C) Volcano plot comparing BRAF-mutated versus

double-wild-type glioblastomas. A larger set of significantly upregulated genes is observed in BRAF-mutated tumors, with comparatively fewer downregulated transcripts, reflecting a more pronounced transcriptional divergence. Dashed lines indicate significance thresholds for log2 fold-change and adjusted p value. Highlighted genes represent the most significantly upregulated and downregulated transcripts in each comparison.

**Exploratory DNA methylation profiling and deconvolution analysis**

Genome-wide DNA methylation analysis was performed in TCGA IDH-wild-type glioblastomas comparing *BRAF*-wild-type (n = 151) and *BRAF*-mutated tumors (n = 4), with the latter interpreted as exploratory due to limited sample size. Using a baseline-centered approach (β = 0.5), both groups showed widespread deviations from intermediate methylation states, with CpGs classified as hypermethylated (β > 0.2; FDR < 0.05) or hypomethylated (β < −0.2; FDR < 0.05) (**Fig. 4**). Distributions were broadly symmetric, indicating global methylation rebalancing rather than directional shifts. Gene Ontology enrichment of hypermethylated CpGs highlighted signaling and membrane-associated processes, including cell adhesion, small GTPase signaling, membrane potential regulation, MAPK signaling, and lipid/anion transport, with additional enrichment of protein assembly and tyrosine phosphorylation processes. In *BRAF*-mutated tumors, electrophysiology-related pathways (e.g., potassium transport, action potential) and endocytosis were additionally observed, though interpreted cautiously given n = 4. Hypomethylated CpGs were enriched for developmental and neurobiological programs, including epithelial morphogenesis, embryonic development, Wnt signaling, and neural processes such as axonogenesis, synaptic function, and neuron projection development. *BRAF*-mutated tumors showed a similar pattern with additional enrichment of embryonic patterning terms (**Supplementary Fig. S11-S14)**. Methylation-based deconvolution indicated a higher cortical neuron score in *BRAF*-mutated tumors (median 0.428) compared to *BRAF*-wild-type tumors (median 0.402), consistent with the enrichment of neurodevelopmental signatures, although this finding remains hypothesis-generating due to the small sample size (n = 4). Collectively, these exploratory data suggest that *BRAF*-mutated IDH-wild-type glioblastomas may retain a stronger differentiation-associated or neural epigenetic component, consistent with their distinct transcriptional profile.

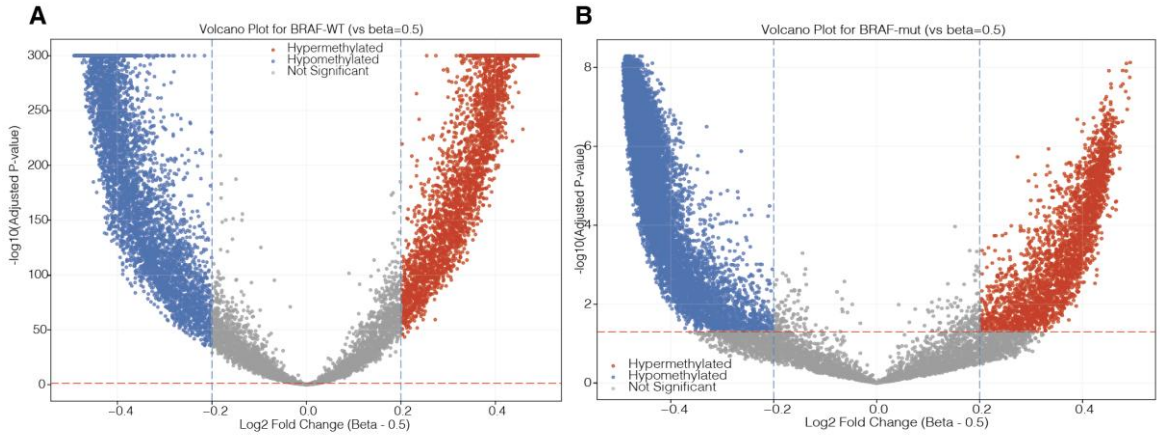



**Figure 4. Genome-wide DNA methylation profiles in BRAF-mutated and BRAF-wild-type glioblastomas.**

(A) Volcano plot of differential methylation relative to the intermediate methylation baseline (β = 0.5) in BRAF-wild-type IDH-wild-type glioblastomas. CpG sites are classified as hypermethylated (red) or hypomethylated (blue) based on deviation from β = 0.5 and statistical significance. A broad and symmetric distribution of hyper- and hypomethylated loci is observed, indicating widespread methylation remodeling. (B) Corresponding analysis in BRAF-mutated glioblastomas. A similar global pattern of balanced hyper- and hypomethylation is observed, consistent with genome-wide reorganization rather than a directional shift in methylation state. Dashed vertical lines indicate effect size thresholds (Δβ), and the horizontal dashed line indicates the adjusted p-value significance cutoff. Gray points represent non-significant CpGs.

**Discussion**

In this integrated analysis of IDH-wildtype glioblastoma across multiple public genomic cohorts, we compared tumors harboring BRAF or PTPN11 mutations with a double-wildtype reference group. We observed no significant differences in age, sex distribution, or overall survival between subgroups, indicating that these mutations alone do not define clinically distinct entities in aggregated datasets. While limited subgroup sizes may reduce sensitivity for small prognostic effects, these findings align with the broader understanding that glioblastoma outcome is governed by multifactorial determinants, including treatment and established molecular markers, which are incompletely captured in public cohorts [14, 15]. In contrast, multi-layer molecular analyses revealed clear differences in genomic and transcriptional architecture. Both BRAF- and PTPN11-mutant tumors were characterized by MAPK-dominant signaling relative to double-wildtype glioblastoma, which is typically driven by upstream receptor tyrosine kinase alterations such as EGFR [14, 16]. PTPN11-mutant tumors showed particularly strong enrichment of RTK-RAS-MAPK signaling, accompanied by additional activation of PI3K-AKT-mTOR and cell cycle pathways. The marked co-occurrence of NF1 alterations in this subgroup supports a model of convergent dysregulation along the RAS/MAPK axis, rather than simple pathway redundancy [17, 18]. BRAF-mutant tumors exhibited a distinct pattern. Although MAPK signaling was enriched, co-alterations were more diffuse and additional canonical pathways were not consistently activated. This likely reflects the functional heterogeneity of BRAF alterations, which differ in RAS dependence and biological behavior [19, 20]. Mixed BRAF classes and potential overlap with related histo-molecular entities may therefore dilute a unified co-mutation signature while preserving pathway-level activation. Notably, prior studies suggest that BRAF-mutant glioblastomas can display distinct biological features despite inconsistent survival associations [15, 20]. Transcriptomic analyses provided the clearest separation between subgroups. BRAF-mutant tumors demonstrated strong enrichment of proliferative, inflammatory, angiogenic, and metabolic programs, consistent with a globally “hyper-activated” transcriptional state [21]. This suggests that BRAF-driven glioblastomas may occupy distinct cellular and microenvironmental states. Preclinical evidence supports this interpretation, linking MAPK perturbation to cell-state transitions and immune evasion, and providing a rationale for combined targeted and immunotherapeutic strategies in BRAF-mutant glioma [22]. Several aspects of the mutational landscape require careful interpretation. Frequently mutated large genes such as TTN and MUC16 likely reflect tumor mutational burden rather than functional driver events [23]. Likewise, the presence of hypermutated outliers, particularly within the PTPN11-mutant cohort, may reflect therapy-

associated evolution, such as temozolomide-induced mismatch repair deficiency [24, 25]. These factors highlight the importance of considering treatment context and mutation burden when interpreting co-alteration patterns in public datasets. From a translational perspective, these findings refine the role of MAPK alterations in glioblastoma. BRAF p.V600E-mutant tumors represent a clinically actionable subgroup, with evidence supporting combined BRAF/MEK inhibition in recurrent disease [20, 26, 27]. However, therapeutic implications vary by BRAF alteration class, emphasizing the need for functional stratification. For PTPN11/SHP2, the clinical relevance remains emerging: preclinical studies indicate roles in both MAPK signaling and immune regulation, and early-phase inhibitors are under development [28, 29], but evidence in glioblastoma remains limited and hypothesis-generating [30]. Exploratory methylation analyses suggested broadly similar global methylation distributions between BRAF-mutant and wildtype tumors, with enrichment of neurodevelopmental and signaling-associated processes. However, given the very small number of BRAF-mutant samples, these findings require validation in larger, well-annotated cohorts. In summary, BRAF- and PTPN11-mutant glioblastomas define MAPK-centric subgroups with distinct genomic and transcriptional architectures rather than discrete prognostic entities. BRAF-mutant tumors are characterized by a globally activated transcriptional state, whereas PTPN11-mutant tumors exhibit strong coupling to RTK-RAS-MAPK signaling with broader pathway co-activation. These findings support a framework in which MAPK-defined glioblastomas represent heterogeneous evolutionary trajectories and underscore the importance of pathway-informed stratification for future therapeutic development.

## Declarations


### Funding

No funding was received for this study.


### Ethics approval and consent to participate

This study used only de-identified, publicly available data from cBioPortal and TCGA and did not involve any newly performed experiments on human participants, human tissue samples, or animals by the authors. All methods were carried out in accordance with relevant guidelines and regulations. Ethical approval and informed consent were obtained in the original studies by the respective contributing institutions and are covered by the policies of the source databases.

**Ethics and Consent to Participate declarations:** not applicable.

### References


1. Aboubakr, O., et al., *Long-term survivors in 976 supratentorial glioblastoma, IDH-wildtype patients.* J Neurosurg, 2025. **142**(1): p. 174–186.
2. Arrieta, V.A., et al., *ERK1/2 phosphorylation predicts survival following anti-PD-1 immunotherapy in recurrent glioblastoma.* Nat Cancer, 2021. **2**(12): p. 1372–1386.
3. Pearson, G., et al., *Mitogen-activated protein (MAP) kinase pathways: regulation and physiological functions.* Endocr Rev, 2001. **22**(2): p. 153–83.
4. Chen, X., et al., *Tyrosine phosphatase PTPN11/SHP2 in solid tumors - bull's eye for targeted therapy?* Front Immunol, 2024. **15**: p. 1340726.
5. Asmamaw, M.D., et al., *A comprehensive review of SHP2 and its role in cancer.* Cell Oncol (Dordr), 2022. **45**(5): p. 729–753.

6. Otani, R., et al., *PTPN11 variant may be a prognostic indicator of IDH-wildtype glioblastoma in a comprehensive genomic profiling cohort.* J Neurooncol, 2023. **164**(1): p. 221–229.
7. Pisapia, P., et al., *BRAF: A Two-Faced Janus.* Cells, 2020. **9**(12).
8. Da, R., et al., *BRAF (AMP) Frequently Co-occurs With IDH1/2, TP53, and ATRX Mutations in Adult Patients With Gliomas and Is Associated With Poorer Survival Than That of Patients Harboring BRAF (V600E).* Front Oncol, 2020. **10**: p. 531968.
9. Ritterhouse, L.L. and J.A. Barletta, *BRAF V600E mutation-specific antibody: A review.* Semin Diagn Pathol, 2015. **32**(5): p. 400–8.
10. McThenia, S.S., et al., *BRAF inhibitor monotherapy in BRAFV600E-mutated pediatric low-grade glioma: a single center's experience.* Front Oncol, 2024. **14**: p. 1505951.
11. Grossauer, S., et al., *Concurrent MEK targeted therapy prevents MAPK pathway reactivation during BRAFV600E targeted inhibition in a novel syngeneic murine glioma model.* Oncotarget, 2016. **7**(46): p. 75839–75853.
12. Dono, A., et al., *Additional genetic alterations in BRAF-mutant gliomas correlate with histologic diagnoses.* J Neurooncol, 2020. **149**(3): p. 463–472.
13. Ramos, M., et al., *Multiomic Integration of Public Oncology Databases in Bioconductor.* JCO Clin Cancer Inform, 2020. **4**: p. 958–971.
14. Brennan, C.W., et al., *The somatic genomic landscape of glioblastoma.* Cell, 2013. **155**(2): p. 462–77.
15. McNulty, S.N., et al., *BRAF mutations may identify a clinically distinct subset of glioblastoma.* Sci Rep, 2021. **11**(1): p. 19999.
16. Cancer Genome Atlas Research, N., *Comprehensive genomic characterization defines human glioblastoma genes and core pathways.* Nature, 2008. **455**(7216): p. 1061–8.
17. Verhaak, R.G., et al., *Integrated genomic analysis identifies clinically relevant subtypes of glioblastoma characterized by abnormalities in PDGFRA, IDH1, EGFR, and NF1.* Cancer Cell, 2010. **17**(1): p. 98–110.
18. Marques, C., et al., *NF1 regulates mesenchymal glioblastoma plasticity and aggressiveness through the AP-1 transcription factor FOSL1.* Elife, 2021. **10**.
19. Owsley, J., et al., *Prevalence of class I-III BRAF mutations among 114,662 cancer patients in a large genomic database.* Exp Biol Med (Maywood), 2021. **246**(1): p. 31–39.
20. Schreck, K.C., et al., *Integrated molecular and clinical analysis of BRAF-mutant glioma in adults.* NPJ Precis Oncol, 2023. **7**(1): p. 23.
21. Liberzon, A., et al., *The Molecular Signatures Database (MSigDB) hallmark gene set collection.* Cell Syst, 2015. **1**(6): p. 417–425.
22. Xing, Y.L., et al., *BRAF/MEK inhibition induces cell state transitions boosting immune checkpoint sensitivity in BRAF(V600E)-mutant glioma.* Cell Rep Med, 2025. **6**(6): p. 102183.
23. Oh, J.H., et al., *Spontaneous mutations in the single TTN gene represent high tumor mutation burden.* NPJ Genom Med, 2020. **5**: p. 33.
24. Choi, S., et al., *Temozolomide-associated hypermutation in gliomas.* Neuro Oncol, 2018. **20**(10): p. 1300–1309.
25. Yip, S., et al., *MSH6 mutations arise in glioblastomas during temozolomide therapy and mediate temozolomide resistance.* Clin Cancer Res, 2009. **15**(14): p. 4622–9.
26. Wen, P.Y., et al., *Dabrafenib plus trametinib in patients with BRAF(V600E)-mutant low-grade and high-grade glioma (ROAR): a multicentre, open-label, single-arm, phase 2, basket trial.* Lancet Oncol, 2022. **23**(1): p. 53–64.
27. Capper, D., et al., *EANO guideline on rational molecular testing of gliomas, glioneuronal, and neuronal tumors in adults for targeted therapy selection.* Neuro Oncol, 2023. **25**(5): p. 813–826.
28. Zhao, M., et al., *SHP2 inhibition triggers anti-tumor immunity and synergizes with PD-1 blockade.* Acta Pharm Sin B, 2019. **9**(2): p. 304–315.
29. Christofides, A., et al., *SHP-2 and PD-1-SHP-2 signaling regulate myeloid cell differentiation and antitumor responses.* Nat Immunol, 2023. **24**(1): p. 55–68.
30. Falchook, G., et al., *A first-in-human phase 1 study of the SHP2 inhibitor BBP-398 in patients with advanced solid tumors.* NPJ Precis Oncol, 2026.

**Supplement**

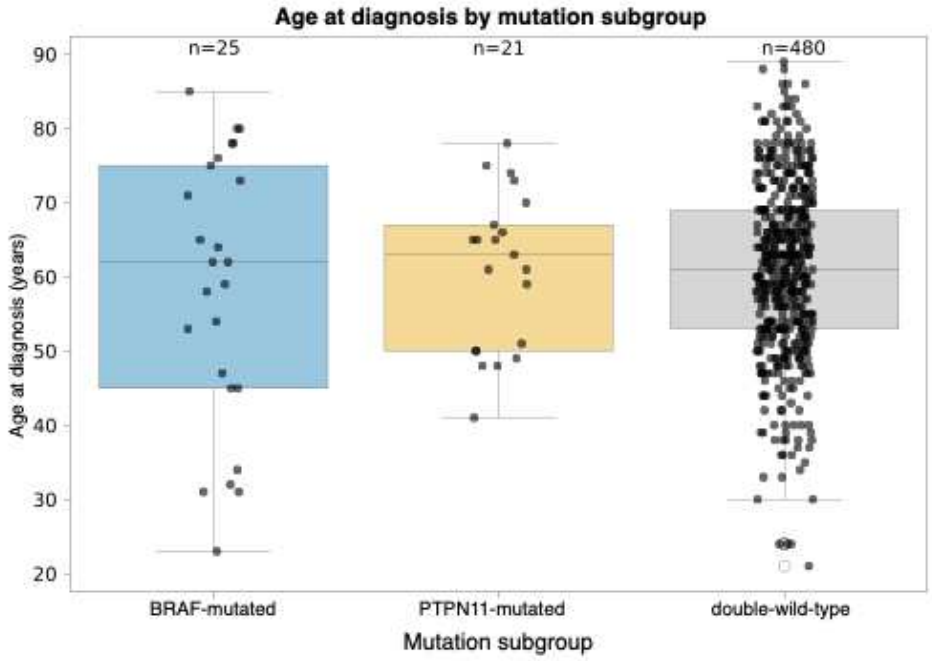



***Figure S1: Age at diagnosis in BRAF-mutated, PTPN11-mutated and BRAF/PTPN11 double-wild-type IDH-wild-type glioblastoma.*** *Boxplots show median and IQR of age at diagnosis in BRAF-mutated (n = 25), PTPN11-mutated (n = 21) and BRAF/PTPN11 double-wild-type (n = 480) IDH-wild-type glioblastoma. Individual patients are shown as jittered points.*

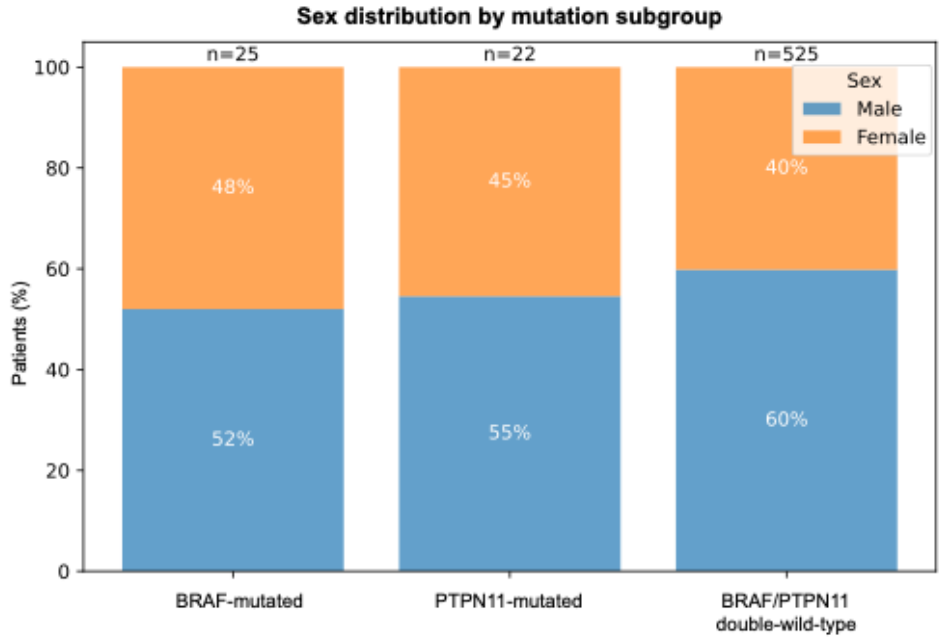



***Figure S2: Sex distribution by BRAF/PTPN11 mutation subgroup in IDH-wild-type glioblastoma.*** *Stacked 100% barplots show the proportion of male and female patients in the BRAF-mutated (n = 25), PTPN11-mutated (n = 22) and BRAF/PTPN11 double-wild-type (n = 525) IDH-wild-type glioblastoma subgroups. Percentages are indicated within each bar.*

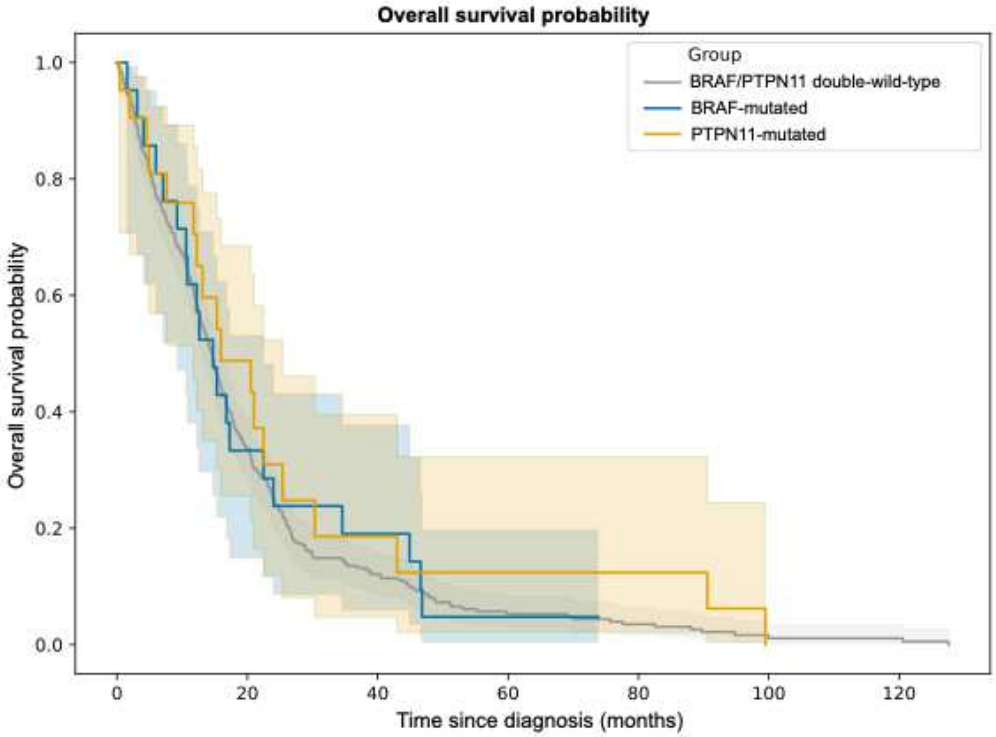
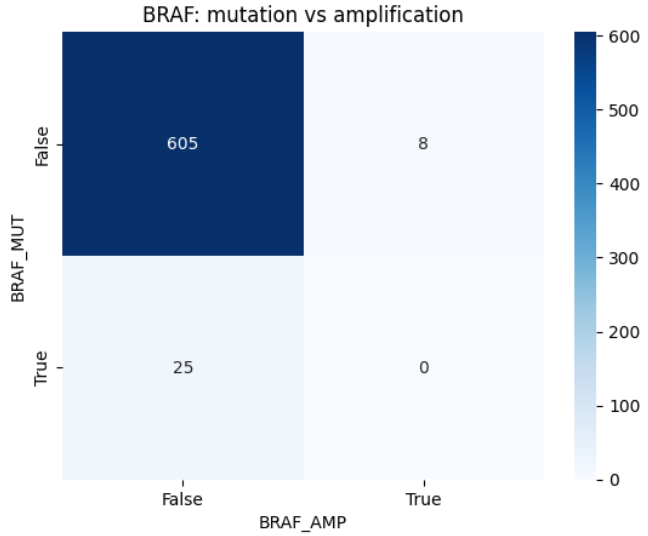
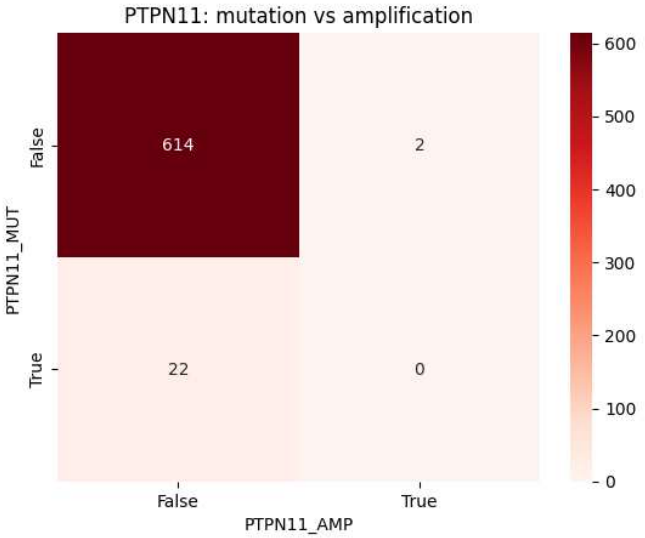



***Figure S3: Overall survival by BRAF/PTPN11 mutation subgroup in IDH-wild-type glioblastoma.*** *Kaplan–Meier curves show overall survival for patients with BRAF-mutated (n = 21), PTPN11-mutated (n = 22) and BRAF/PTPN11 double-wild-type (n = 448) IDH-wild-type glioblastoma. Shaded areas indicate 95% confidence intervals. Survival distributions did not differ significantly between subgroups (global log-rank p = 0.60).*

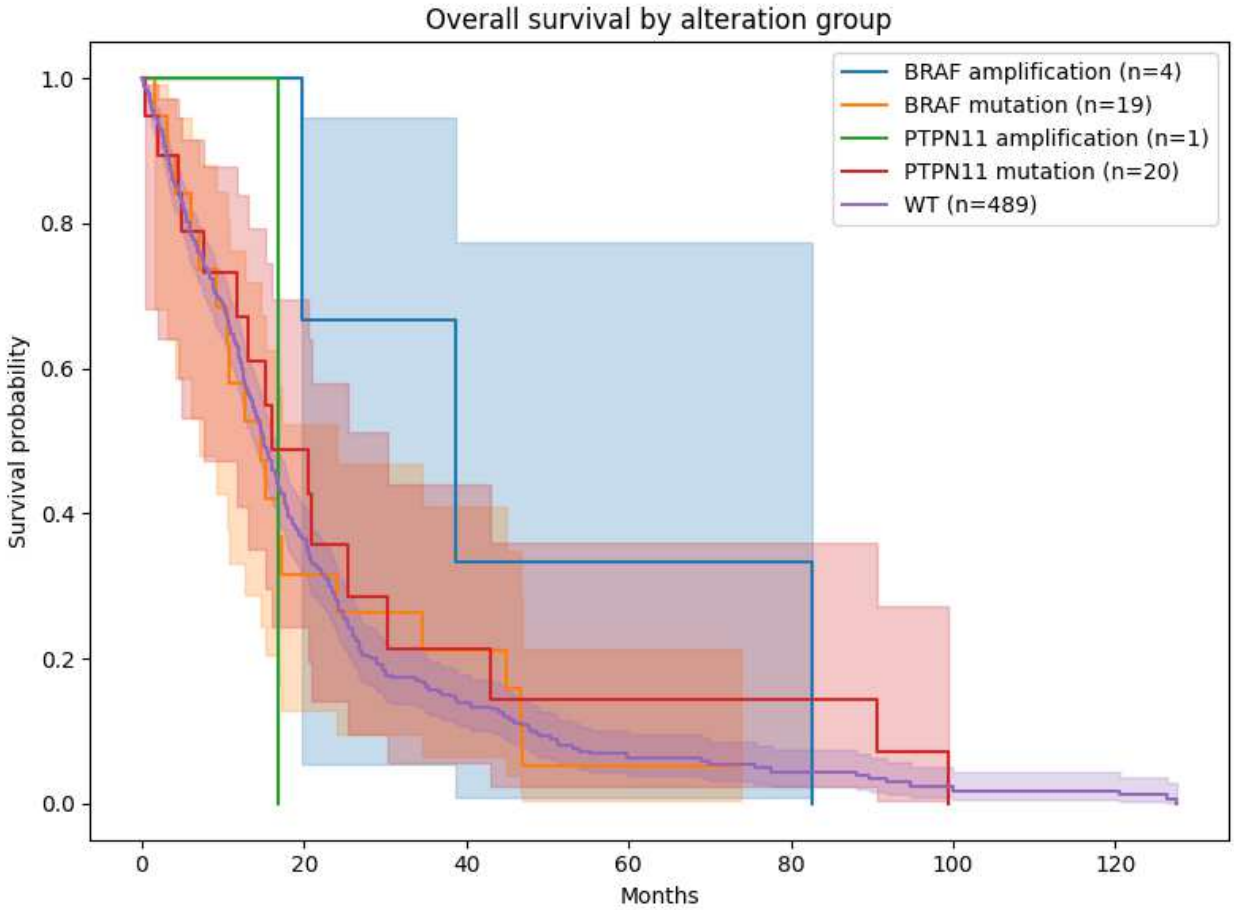



***Supplementary Figure S4: Relationship between BRAF mutation and BRAF amplification.*** *Heatmap of patient counts cross-classifying BRAF mutation status (mutated vs non-mutated) and BRAF amplification status (amplified vs non-amplified).*

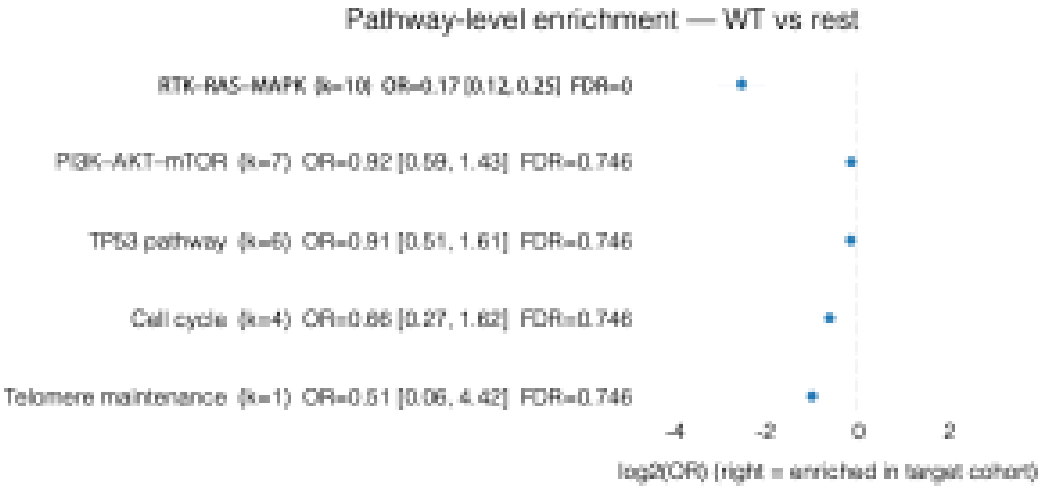



an

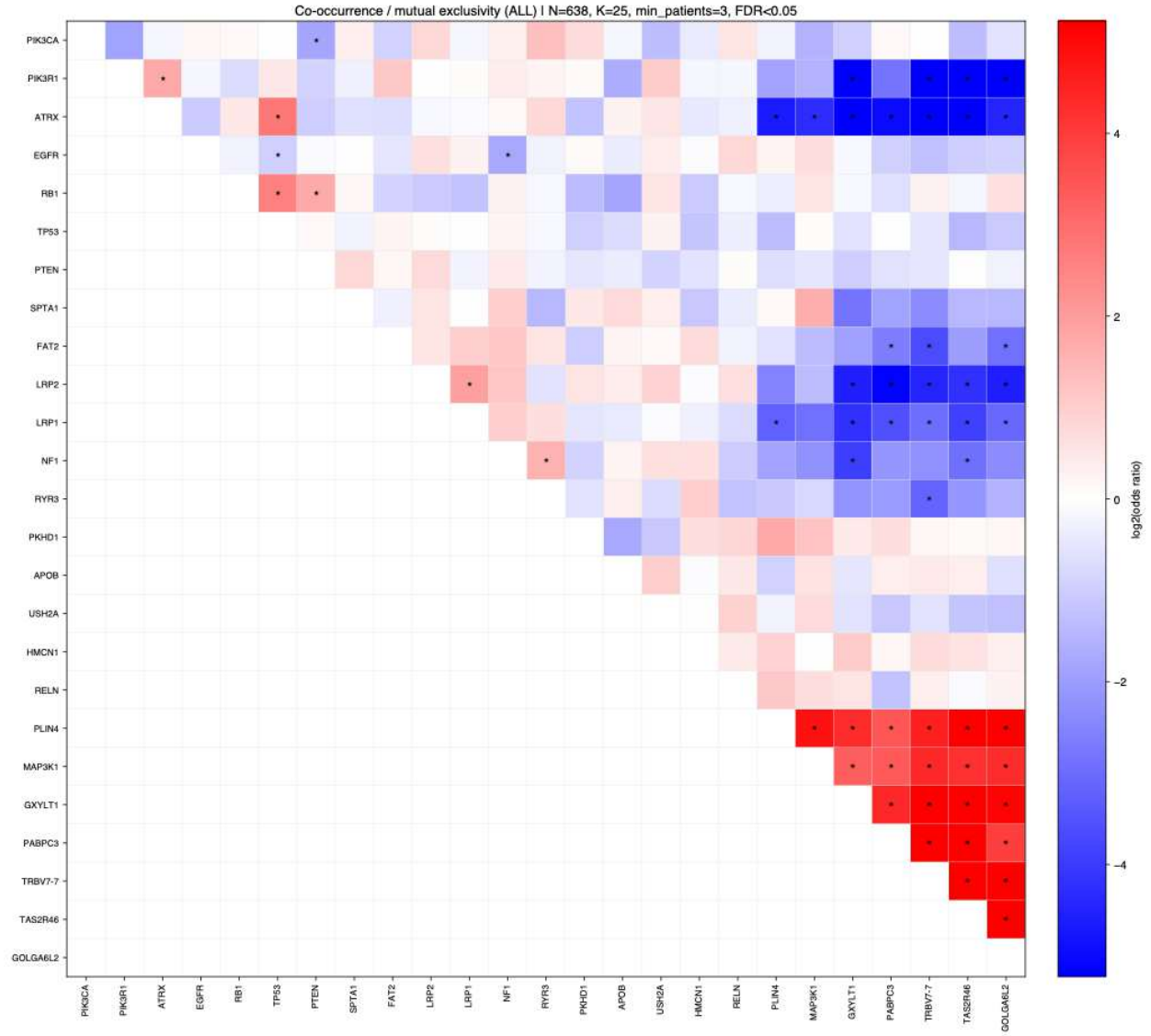
***Supplementary Figure S5: Relationship between PTPN11 mutation and PTPN11 amplification.***




***Supplementary Figure S6: Overall survival by alteration group (mutation or amplification).*** *Kaplan–Meier curves for groups defined as BRAF-mutated, PTPN11-mutated, BRAF-amplified only, PTPN11-amplified only and double-wild-type.*

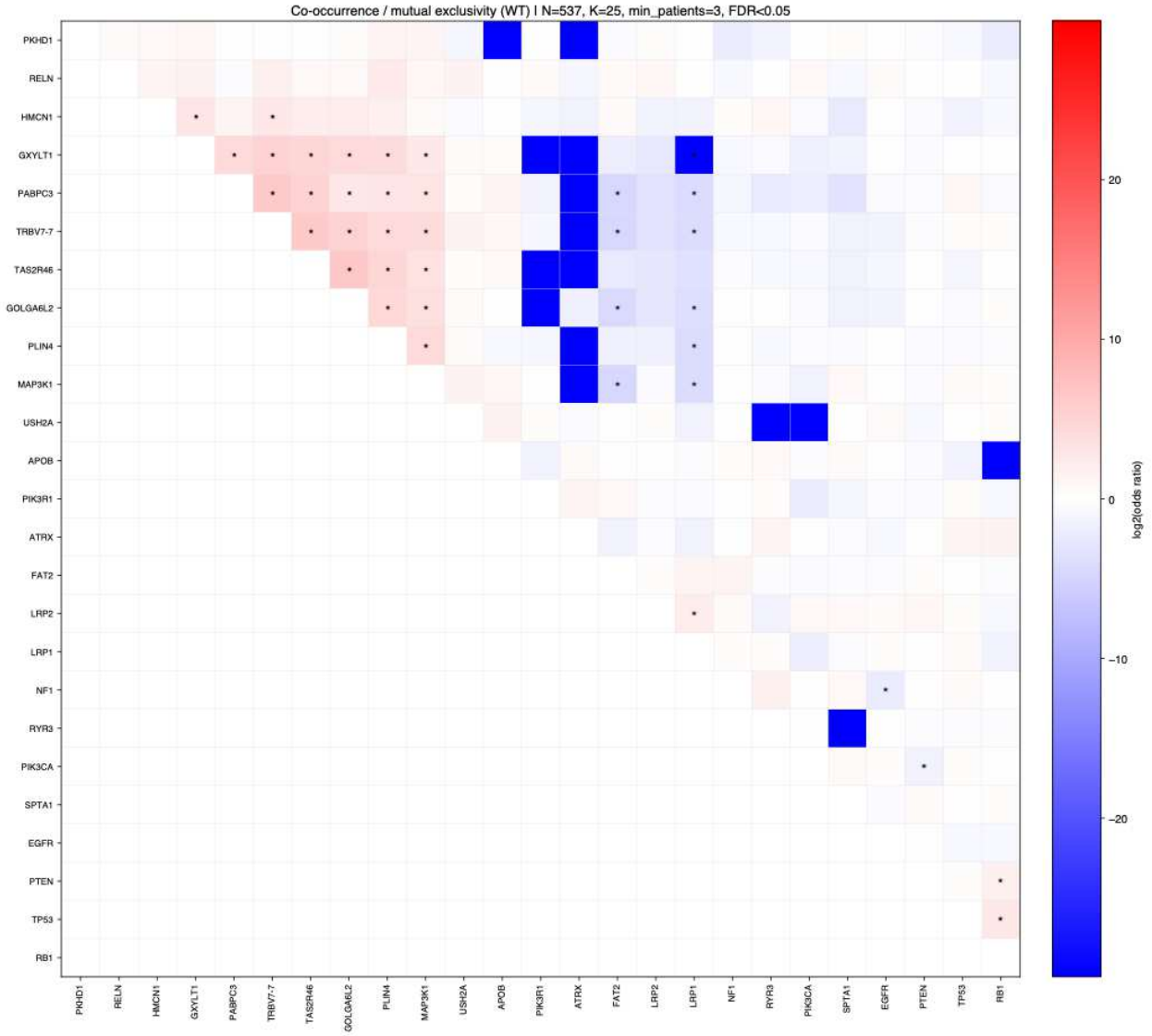



***Supplementary Figure S7: Pathway-level enrichment analysis comparing double-wild-type glioblastomas with the remaining genomic subgroups.*** *Forest plot showing pooled pathway-level odds ratios from gene-set enrichment analysis for canonical oncogenic pathways in double-wild-type glioblastomas versus all other tumors. Points indicate log2(OR) and horizontal lines represent 95% confidence intervals. Negative values indicate depletion in the double-wild-type cohort, whereas positive values indicate enrichment.*

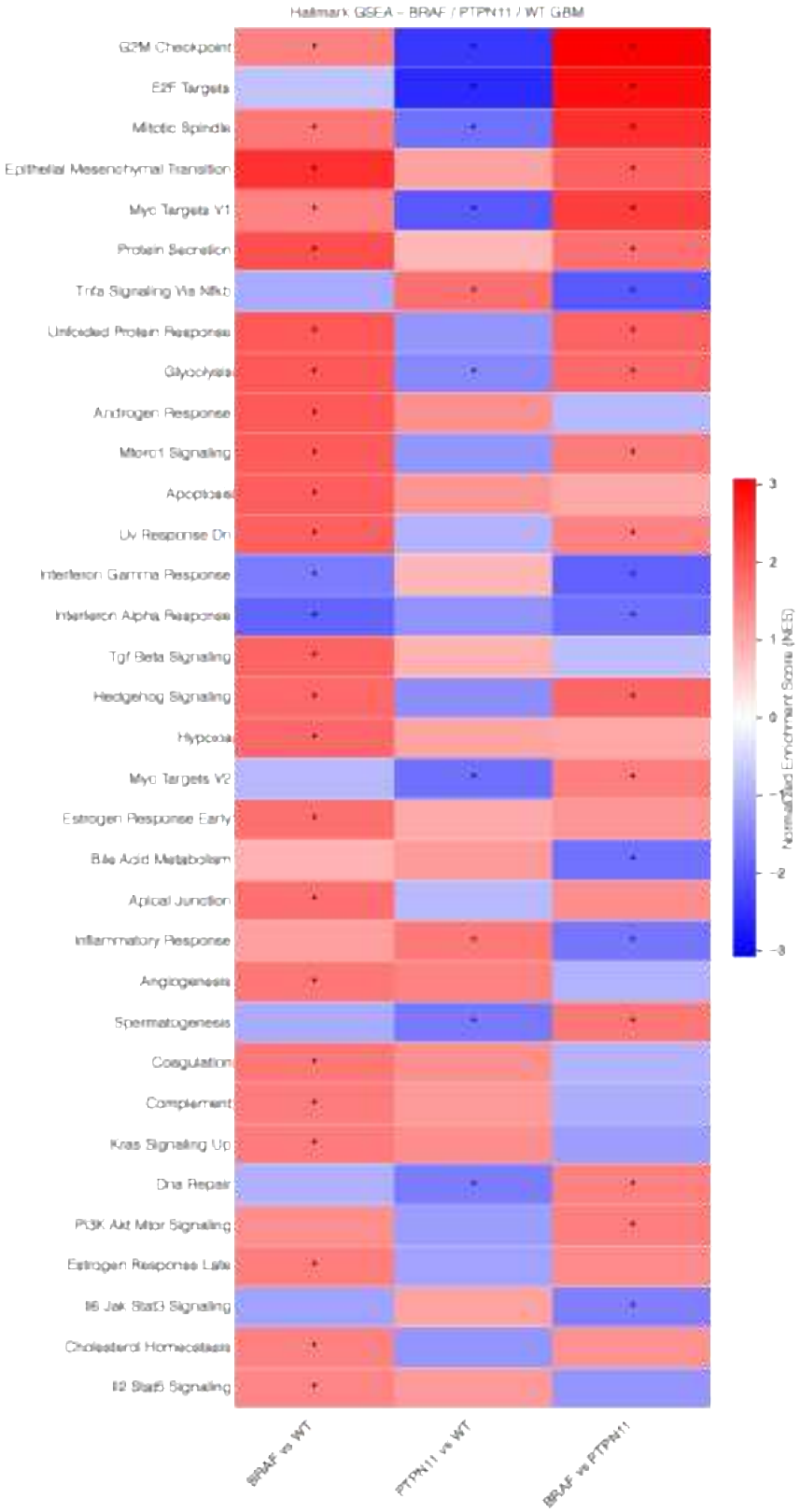



***Supplementary Figure S8: Pairwise co-occurrence and mutual exclusivity analysis of recurrently altered genes across all IDH-wild-type glioblastomas.*** *Heatmap showing mutation-burden-adjusted pairwise associations among recurrently altered genes in the combined cohort. Color indicates log2(odds ratio), with red*

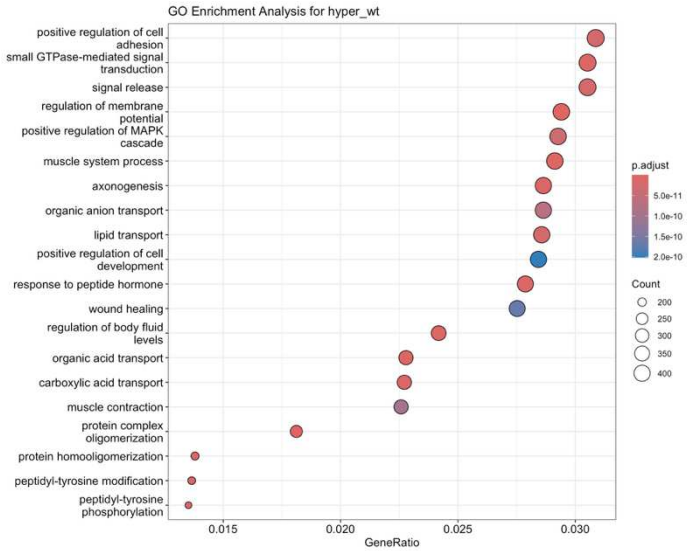
*denoting co-occurrence and blue denoting mutual exclusivity. Dots mark associations significant after FDR correction.*



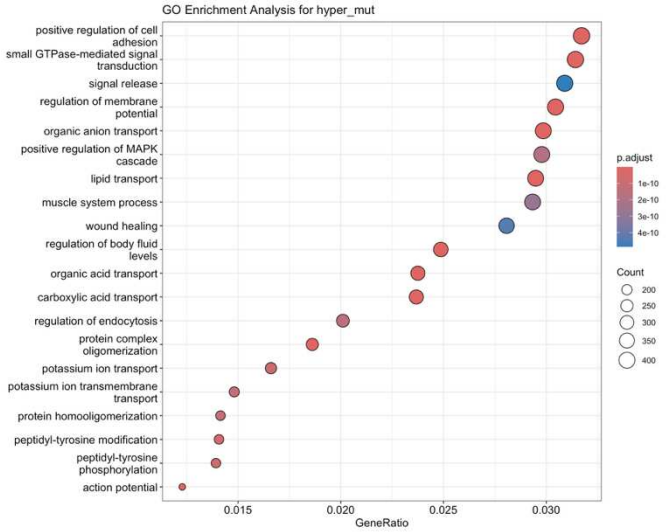

***Supplementary Figure S9: Pairwise co-occurrence and mutual exclusivity analysis of recurrently altered genes in double-wild-type IDH-wild-type glioblastomas.*** *Heatmap showing mutation-burden-adjusted pairwise associations among recurrently altered genes within the double-wild-type cohort. Color indicates log2(odds ratio), with red denoting co-occurrence and blue denoting mutual exclusivity. Dots mark associations significant after FDR correction.*



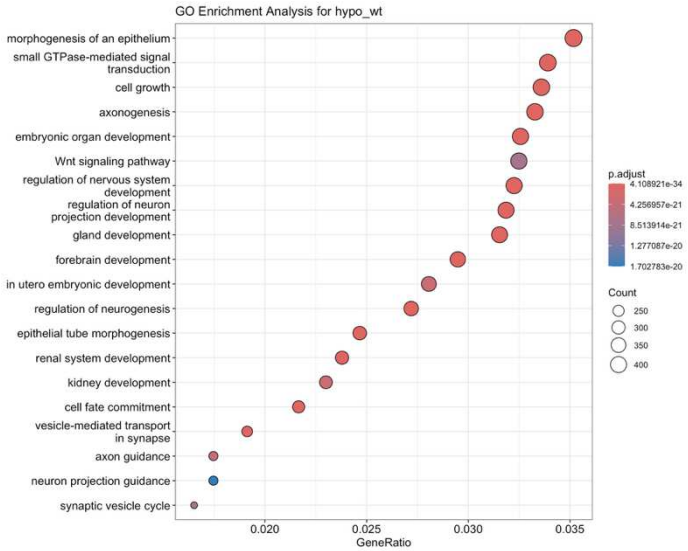

***Supplementary Figure S10: Preranked Hallmark gene set enrichment analysis across glioblastoma subgroups.*** *Heatmap showing normalized enrichment scores (NES) for Hallmark pathways from preranked GSEA in the three pairwise comparisons: BRAF-mutated vs double-wild-type, PTPN11-mutated vs double-wild-type, and BRAF-mutated vs PTPN11-mutated glioblastomas. Red indicates positive enrichment in the first group of each comparison, whereas blue indicates relative depletion. Dots indicate significantly enriched gene sets.*



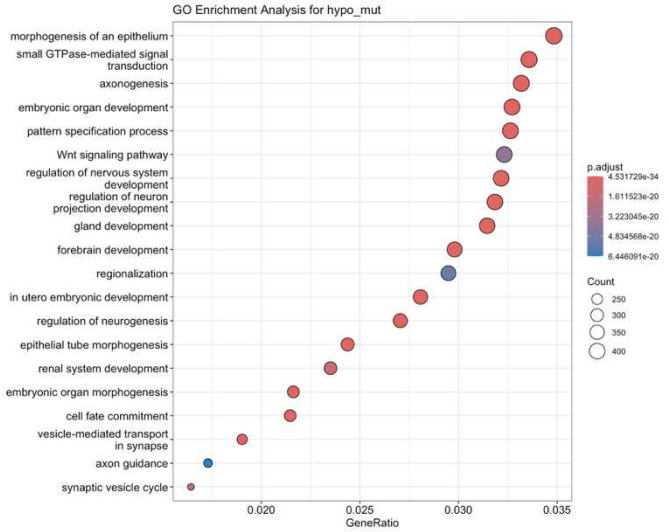

***Supplementary Figure S11: Gene Ontology enrichment analysis of genes annotated to hypermethylated CpGs in BRAF-wild-type IDH-wild-type glioblastomas.*** *Dot plot showing the top enriched Biological Process terms for genes linked to hypermethylated CpGs identified in the BRAF-wild-type group. Dot size indicates gene count, dot position indicates gene ratio, and color represents adjusted p values.*




***Supplementary Figure S12: Gene Ontology enrichment analysis of genes annotated to hypermethylated CpGs in BRAF-mutated IDH-wild-type glioblastomas.*** *Dot plot showing the top enriched Biological Process terms for genes linked to hypermethylated CpGs identified in the BRAF-mutated group. Dot size indicates gene count, dot position indicates gene ratio, and color represents adjusted p values.*




***Supplementary Figure S13: Gene Ontology enrichment analysis of genes annotated to hypomethylated CpGs in BRAF-wild-type IDH-wild-type glioblastomas.*** *Dot plot showing the top enriched Biological Process terms for genes linked to hypomethylated CpGs identified in the BRAF-wild-type group. Dot size indicates gene count, dot position indicates gene ratio, and color represents adjusted p values.*




***Supplementary Figure S14: Gene Ontology enrichment analysis of genes annotated to hypomethylated CpGs in BRAF-mutated IDH-wild-type glioblastomas.*** *Dot plot showing the top enriched Biological Process terms for genes linked to hypomethylated CpGs identified in the BRAF-mutated group. Dot size indicates gene count, dot position indicates gene ratio, and color represents adjusted p values.*

| Comparison | Test | n (per group) | p (raw) | p (Holm-adjusted) |
|---|---|---|---|---|
| BRAF-mutated vs PTPN11-mutated vs double-wild-type | Kruskal–Wallis | 25 / 21 / 480 (BRAF / PTPN11 / double-wild-type) | 0.95 | n.a. |
| BRAF-mutated vs double-wild-type | Mann–Whitney U | 25 / 480 | 0.75 | 1 |
| PTPN11- mutated vs double-wild-type | Mann–Whitney U | 21 / 480 | 0.94 | 1 |
| BRAF-mutated vs PTPN11-mutated | Mann–Whitney U | 25 / 21 | 0.84 | 1 |

***Supplementary Table S1: Global and pairwise tests for age at diagnosis by mutation subgroup in IDH-wild-type glioblastoma.*** *Data shown for IDH-wild-type glioblastoma only, excluding patients with concurrent BRAF and PTPN11 mutations.*

| Sex | BRAF-mutated | PTPN11-mutated | Double-wild-type |
|---|---|---|---|
| n | (n = 25) | (n = 22) | (n = 525) |
| Male | 13 (52%) | 12 (55%) | 314 (60%) |
| Female | 12 (48%) | 10 (45%) | 211 (40%) |

***Supplementary Table S2: Sex distribution by BRAF/PTPN11 mutation subgroup in IDH-wild-type glioblastoma.*** *Data shown for patients with available sex information. p value from chi-square test of independence across the three subgroups ($\chi^2(2) = 0.81$, $p = 0.67$).*

| Subgroup | n | Deaths | Censored | Median OS (months)* |
|---|---|---|---|---|
| BRAF-mutated | 21 | 20 | 1 | 14.7 |
| PTPN11-mutated | 22 | 18 | 4 | 16 |
| BRAF/PTPN11 double-wild-type | 448 | 368 | 80 | 14.5 |

***Supplementary Table S3: Overall survival by BRAF/PTPN11 mutation subgroup in IDH-wild-type glioblastoma.***
**Median overall survival estimated from Kaplan–Meier curves.*

| Comparison | Test | p value |
|---|---|---|
| BRAF-mutated vs BRAF/PTPN11 double-wild-type | Log-rank (pairwise) | 0.78 |
| PTPN11-mutated vs BRAF/PTPN11 double-wild-type | Log-rank (pairwise) | 0.32 |
| BRAF-mutated vs PTPN11-mutated | Log-rank (pairwise) | 0.62 |
| BRAF-mutated vs PTPN11-mutated vs double-wild-type | Global log-rank | 0.6 |

***Supplementary Table S4: Log-rank tests comparing overall survival by BRAF/PTPN11 mutation subgroup in IDH-wild-type glioblastoma.*** *All p values two-sided. No adjustment for multiple testing was applied to survival comparisons because no trend toward significance was observed.*

| ok and now this sheet 5? | BRAF-amplified samples (n) | PTPN11-amplified samples (n) | Samples with both genes amplified (n) |
|---|---|---|---|
| gbm_cptac_2021 | 3 | 1 | 0 |
| gbm_mayo_pdx_sarkaria_2019 | 0 | 0 | 0 |
| gbm_tcga | 7 | 2 | 0 |
| gbm_tcga_pan_can_atlas_2018 | 9 | 1 | 0 |
| gbm_tcga_pub2013 | 8 | 2 | 1 |

***Supplementary Table S5: Availability of copy-number data and counts of BRAF and PTPN11 amplifications by study.*** *Amplification was defined as a discrete copy-number value of +2 in cBioPortal GISTIC-style CNA data.*

| Gene | Amplified tumour samples (n) | Unique patients (n) |
|---|---|---|
| BRAF | 27 | 8 |
| PTPN11 | 6 | 2 |

***Supplementary Table S6: Samples and unique patients with BRAF or PTPN11 amplification across all studies.*** *Counts are aggregated across all cBioPortal glioblastoma studies with available copy-number data.*